IEEE Access
Multidisciplinary | Rapid Review | Open Access Journal

Received April 9, 2019, accepted April 23, 2019, date of publication April 30, 2019, date of current version May 13, 2019.

Digital Object Identifier 10.1109/ACCESS.2019.2914075

Numerical Investigation on Collision of Pollution Particles on Outdoor Insulators

YONG LIU[1], (Member, IEEE), XIANGHUAN KONG[1], (Student Member, IEEE), BOXUE DU[1], (Senior Member, IEEE), JIN LI[1], (Member, IEEE), AND JINGSHENG SUN[2]

[1]School of Electrical and Information Engineering, Tianjin University, Tianjin 300072, China
[2]State Grid Tianjin Power Electric Corporation, Tianjin 300010, China

Corresponding author: Yong Liu (tjuliuyong@tju.edu.cn)

This work was supported in part by the National Nature Science Foundation of China under Grant 5167718, in part by the Youth Fund of National Natural Science Foundation of China under Grant 51807136, in part by the Natural Science Foundation, Tianjin, under Grant 18JCQNJC07300, and in part by the Science and Technology Project of State Grid Corporation of China under Grant 5202011600UV.

ABSTRACT Accumulation of pollution particles on outdoor insulators is the premise of pollution flashover accidents in power systems. In this paper, according to the actual operating polymer insulators, the wind velocity, the concentration of pollution particles, the diameter of pollution particles, and the hanging angle of insulator were considered to investigate the accumulation characteristic of pollution particles by using FLUENT software. The pressure nephogram of polymer insulator, the velocity vector of air flow field, movement trajectory of pollution particles, and collision rate were obtained. It is found that the pressure of the insulator surface on the windward side is bigger than that on the leeward side, and the pressure difference increases with increasing the wind velocity. As the increase in particle diameter, the collision rate between pollution particles and insulator surface shows the increasing tendency. When the diameter of pollution particles is small, the easier the particles follow the airflow to bypass the insulator surface without colliding with it. However, due to the influence of gravity force and inertia, the collision rate of pollution particles increases significantly with the increase in particle diameter. Under the strong wind velocity, the air swirls are generated on the leeward side of the insulator surface, causing the collision rate of the pollution particles increases slowly with the increase in the wind velocity. While the concentration of pollution particle increases, the collision number between insulator surface and pollution particles shows the increasing tendency at different wind velocity. When the particle diameter is in range of 1 to 8 μm, with increasing the hanging angle of ''V'' type insulator from 0° to 60°, the collision rate of pollution particles shows the increasing tendency. When the particle diameter is 9 to 50 μm, the collision rate of particles shows the increasing tendency when the insulator angle is lower than 30°, but shows the decreasing tendency from 30°to 60°. As the humidity increases, the water vapor in the air prevents the movement of pollution particles, resulting in a decrease in the collision rate. With increasing the pollution particles diameter, the influence of air humidity on the collision rate of pollution particles is gradually weakened.

INDEX TERMS Outdoor insulator, hydromechanics, distribution of flow field, collision rate.

I. INTRODUCTION

Pollution flashover accident is one of the main faults in various high voltage transmission lines, which affects the stability and safety of power systems [1], [2]. In general, the pollution flashover goes through the following four processes: the pollution accumulation, the moisture absorption, the generation of partial discharges, development of partial arc until the completion of flashover. The accumulation of pollution particles on the insulator surface is the premise of the pollution flashover accidents [3]–[6]. Therefore, for the reliability of power grid, it is significant to study the accumulation characteristics of pollution particles and to obtain the movement trajectory of pollution particles around the insulator.

To reduce the pollution flashover accidents of outdoor insulators, the anti-icing polymer insulator has been considered to be applied in the reconstruction of operating transmission line in severely ice-covered areas. The anti-icing

The associate editor coordinating the review of this manuscript and approving it for publication was Bora Onat.

polymer insulator with specifical sheds (larger sheds, large sheds and small sheds exist alternately) are used to replace the traditional polymer insulators. As the structure change, the distance between the electrodes on polymer insulator surface increases significantly, which improves the flashover voltage and reduces the pollution flashover accidents. Drawing a comparison with glass insulators, porcelain insulators and traditional polymer insulators, the shed structure of anti-icing polymer insulator is different, which leads that the air flow field and the accumulation characteristic of pollution particles obviously changes [7]–[9]. In the operating transmission line, there are a variety of suspension methods for polymer insulator, such as ''V'' and ''Λ'' types. The change of the angle between two insulators for these suspension methods affects the accumulation characteristic of pollution particle. Therefore, it is necessary to study the accumulation characteristics of pollution particles on the anti-icing polymer insulator surface.

Nowadays, the accumulation characteristic of pollution particle on outdoor insulators is studied by using natural pollution accumulation test, artificial simulation test and analysis of finite element simulation [10]–[14]. Zhijin *et al.* [10] simulated the accumulation of pollution particles by the Eulerian multiphase model. The air flow field around insulators was calculated and the volume fraction of the particle phase was used to characterize the pollution level of insulator surface. Yukun *et al.* [11] investigated the mechanical mechanism of pollution accumulation on XP13-160 porcelain suspension disc insulators, proposing a discriminant for the deposition on the insulator surface. Gouda *et al.* [12] simulated the polluted insulators of overhead transmission lines in desert environments by using laboratory tests. The effect of conductivity variation on the polluted insulator was found, but the pollution accumulation characteristic was ignored. Baker *et al.* [13] compared the surface degradation of insulators in harsh marine pollution environment from different materials including silicone rubber, ethylene propylene diene monomer and high-density polyethylene. Chuyan *et al.* [14] built a testing apparatus to simulate the deposition characteristic of pollution particles in fog-haze environment by using three type insulators. The relationship between the equivalent salt deposit density and PM 2.5 was investigated.

In this paper, the finite element model of polymer insulator and air flow field were established by using FLUENT software. Considering the influences of air flow field and gravity field, the gas-solid two-phase flow method of simulation theory was used to investigate the motion trajectory and accumulation characteristics of pollution particles. The influence factors including the wind level, the pollution particle concentration, the diameter of pollution particles, the air humidity and the hanging angle of outdoor insulators were analyzed. The pressure of insulator surface, the velocity vector of air flow field around polymer insulator, trajectory of pollution particles and collision rate between insulator surface and pollution particles were investigated to reveal the pollution accumulation characteristics on outdoor insulator.

II. MODEL ESTABLISHMENT AND SIMULATION METHODS

A. THE FORCE ANALYSIS OF POLLUTION PARTICLE

The movement of pollution particles around the insulator is affected by electrical field, air flow field and gravity field. The force type applied to the pollution particles has a great relationship with the particle diameter. When the particle diameter is less than 1 μm, the main motion of the particles is Brownian motion, and the path of particles in Brownian motion is erratic and frequently changes the direction. When the particle size is larger than 1 μm, the way to affect particle transport is the turbulent diffusion, which is an extraordinarily complex three-dimensional flow [15]. The pollution particles with different diameters move into the atmosphere under the influence of the ascending airflow. When the particles reach a certain height, they will transmit laterally under the influence of horizontal drag force. The height of 500 kV insulators is about 20 meters from the ground, and the pollution particle size around the insulator is about 50 μm [16]. Therefore, based on the distribution range of pollution particle diameter around the insulator and the suspension height of the insulator, the force of pollution particles can be divided into three types: the electrical force, the fluid drag force and the gravity force. The forces of pollution particles around polymer insulator are shown in Figure 1, where F_1 is the fluid drag force, F_2 is the electrical force, G is the gravity force. As the electrical force is very weak, it can not influence the movement path of pollution particles, but can make particles attach to the insulator surface more firmly [17]. This paper focused on the collision rate and movement trajectory of pollution particles where the influence of electrical force was ignored.

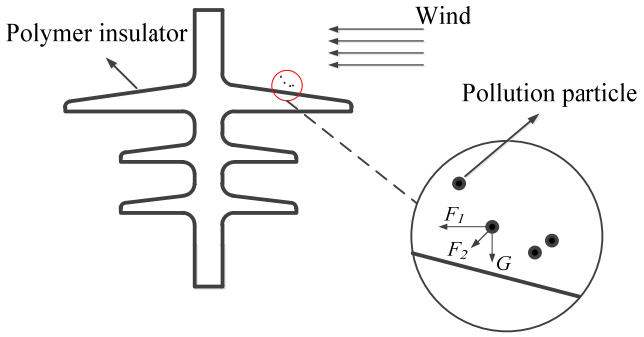

FIGURE 1. Forces of pollution particles around the insulator.

B. TURBULENCE HYDRODYNAMIC MODEL AND GAS-SOLID TWO-PHASE FLOW MODEL

Air turbulence is an extraordinarily complex three-dimensional flow, which is a disorder and unsteady movement, prevalent in nature. Insulators include complex structures such as sheds and mandrels, which leads to the typical turbulence in the air flow around them [18]. Generally, the numerical simulation and calculation of the turbulence is based on the Reynolds-Averaged turbulence model, which is

time-averaged equations of motion for the fluid flow. The turbulence time-averaged governing equation of incompressible fluid can be expressed as follows:

$$\frac{\partial (u_i)}{\partial x_i} = 0 \tag{1}$$

$$\frac{\partial (\rho u_i)}{\partial t} + \frac{\partial \left(\rho u_i u_j\right)}{\partial x_j} = \rho f_i - \frac{\partial p}{\partial x_i} + \frac{\partial}{\partial x_i}\left(\mu \frac{\partial u_i}{\partial x_j}\right) + \left[-\frac{\partial \left(\rho \overline{u_i' u_j'}\right)}{\partial x_j}\right] \tag{2}$$

where u is the velocity of air fluid in m/s; ρ is fluid density in kg· m^{-3}; p is the fluid pressure; μ is air flow viscosity; f is the mass force per unit mass fluid; x_i, x_j respectively represent three rectangular coordinate components ($i, j = 1, 2, 3$, $i \neq j$); $-\rho \overline{u_i' u_j'}$ is Reynolds Stresse. Reynolds stress is added to the momentum equation after a series of time-averaged treatments of the turbulent instantaneous motion equation using the Reynolds time-averaged method, which results in an increase in the unknown variables of the equation system. Therefore, a new RNG k-ε turbulence model must be used to solve the equations, where k is the kinetic energy of turbulent in $m^2 \cdot s^{-2}$ and ε is the dissipation rate in $m^2 \cdot s^{-3}$. The equations are as follows:

$$\frac{\partial (\rho k)}{\partial t} + \frac{\partial (\rho k u_i)}{\partial x_i} = \frac{\partial}{\partial x_j}\left[\alpha_k \left(\mu + \rho C_\mu \frac{k^2}{\varepsilon}\right) \frac{\partial k}{\partial x_j}\right] + G_k - \rho\varepsilon \tag{3}$$

$$\frac{\partial (\rho \varepsilon)}{\partial t} + \frac{\partial (\rho \varepsilon u_i)}{\partial x_i} = \frac{\partial}{\partial x_j}\left[\alpha_\varepsilon \left(\mu + \rho C_\mu \frac{k^2}{\varepsilon}\right) \frac{\partial \varepsilon}{\partial x_j}\right] + C_{1\varepsilon}^* \frac{\varepsilon}{k} G_k - C_{2\varepsilon} \rho \frac{\varepsilon^2}{k} \tag{4}$$

where G_k is the turbulent energy caused by the velocity gradient in kg · m^{-1} · s^{-3}, C_μ is the empirical constant of 0.0845, $C_{1\varepsilon}^*$ contains the time-averaged strain rate of the main fluid flow, $C_{2\varepsilon}$ is the constant coefficient of 1.68.

When the pollution particles are added to the air flow field in the simulation experiment, the fluid medium changes from one phase to two phases, which makes the gas-solid two-phase flow method is applied to simulate the movement trajectory of pollution particles. Pollution particles in air flow field are discrete, so the Euler-Lagrange Approach is used to calculate the discrete phase. In the FLUENT software, the trajectory of discrete phase particle is calculated by the differential equation of the forces in the Lagrangian coordinate system. The force equation of the particle is in the Cartesian coordinate system, as shown in Equation (5), and the direction is along the X axis direction [11].

$$\frac{du_p}{dt} = \frac{18\mu}{\rho_p d_p} \cdot \frac{C_D}{24}(u - u_p) + \frac{g_x(\rho_p - \rho)}{\rho_p} \tag{5}$$

where u is the velocity of air fluid in m/s, u_p is the velocity of pollution particles in m/s, g_x is gravitational acceleration in m·s^{-2}, ρ_p is particle density in kg/m^3, μ is air fluid viscosity, d_p is the diameter of pollution particles in m, C_D is the drag force coefficient of the fluid, which can be expressed by the Reynolds number [19].

$$C_D = \alpha_1 + \frac{\alpha_2}{Re} + \frac{\alpha_3}{Re^2} \tag{6}$$

$$Re = \frac{\rho d_p \left|u - u_p\right|}{\mu} \tag{7}$$

where Re is the Reynolds number, $\alpha_1, \alpha_2, \alpha_3$ change with the Reynolds number.

In this paper, the calculation method of the simulation is a one-way coupling. Firstly, the turbulence model is used to solve the transportation process of the airflow phase, and the distribution of the force and flow field around the insulator is obtained. Then, the particle trajectory model under the Lagrangian coordinate system is used to calculate the trajectory of pollution particles.

C. ESTABLISHMENT OF SIMULATION MODEL

Relevant publications show that the accumulation of pollution particle is affected by various factors such as the fluid drag force and the gravity force [5], [20]. The wind level, the concentration and diameter of pollution particle, and the hanging angle of insulator can also change the characteristic of pollution accumulation. The air around the insulator is set to the continuous phase for the simulation calculation of turbulent fluid, then the pollution particles are added to the air flow field as discrete phase. In this approach, the movement of the flow field is solved firstly, then the obtained flow field is coupled with the discrete phase to calculate the collision rate between insulator surface and pollution particle. The calculation flowchart of Hydrodynamic simulation is shown in Figure 2.

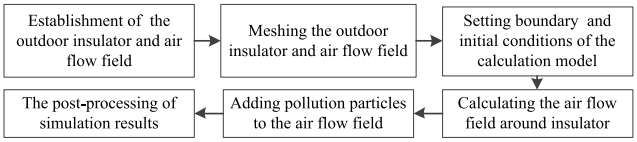

FIGURE 2. Calculation flowchart of Hydrodynamic simulation of pollution particles.

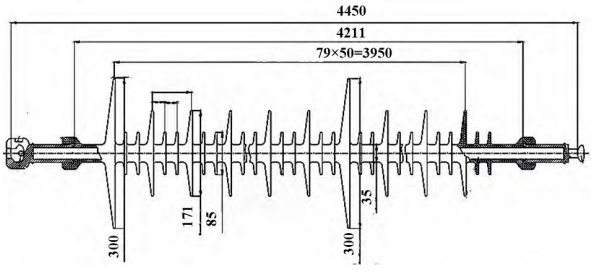

FIGURE 3. The structure and dimension of 500 kV outdoor insulator.

Figure 3 shows the dimension and structure of 500 kV polymer insulator, having the largest shed diameter of 300 mm, creepage distance of 15200 mm and height

of 4450 mm. The insulator sheds are divided into 50 cells and the length of each cell is 79 mm. In order to simplify the calculation model, one cell and half a cell of the insulator was established.

There is a boundary for the space of the flow field in the numerical simulation, so that the air flow at the boundary of flow field will be affected remarkably. To ensure the accuracy of simulation results, the size of air flow field was designed as large as possible. According to the actual operating conditions, the dimension of air flow field was set 2500 mm × 3000 mm × 3500 mm. Figure 4 shows the 3-D model of outdoor insulator and computation region of air flow field. The ''a'' plane of flow flied is defined as the inlet of air and pollution particles. The ''b'' plane of flow field is defined as the outlet of flow.

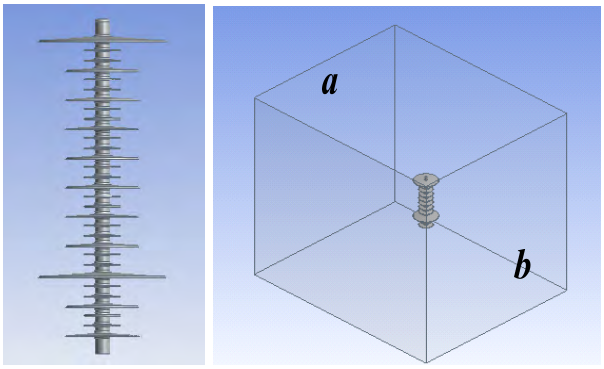

FIGURE 4. The 3-D model of the insulator and computation region of air flow field.

The shape of insulator surface is complicated, and the curvature of insulator surface changes sharply. The size of meshing grid cell is highly correlated with concentration of pollution particles in the post-processing step. Therefore, it is significant to set an appropriate cell size to mesh the insulator and air flow field. In order to accurately mesh the fluid region, the air flow field was divided into 9 parts. The fluid area around the insulator was meshed by the tetrahedral grid cells. The size of tetrahedral grid cell was defined as ''Fine'' and the relevance of grid cell was defined as ''100'' to make grid more accurate. The other regions of flow field were meshed by the hexahedron grid cells. The size of hexahedron grid cell was set as ''Medium'' to reduce the calculation time. Figure 5 shows the mesh result of air flow field and polymer insulator model.

D. SETTING BOUNDARY CONDITION OF SIMULATION

Before using the finite element analysis method to calculate the air flow field, the initial condition and boundary condition of calculation model should be set. The ''a'' plane boundary condition and ''b'' plane were respectively set as the ''inlet surface'' and ''outlet surface'', the other four faces of the air flow field were set as ''wall''. The airflow and pollution particles were injected into the air flow field from a direction perpendicular to the ''a'' plane and ejected from ''b'' plane

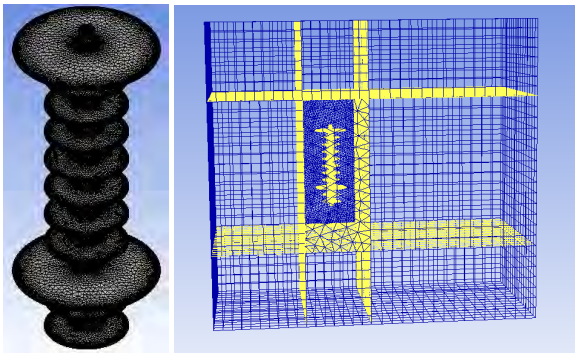

FIGURE 5. The mesh result of air flow field and polymer insulator model.

(Figure 4). When the pollution particles collide with the insulator surface, they will be regarded as ''trap''. When pollution particles collided with ''wall'' and ''outlet surface'', they will be set as ''escape''. The collision rate (P) was defined as the ratio of ''trap'' particles to total particles.

$$P = \frac{N_a}{N} \tag{8}$$

The material property of pollution particles was replaced by Calcium Carbonate ($CaCO_3$) in the sphere shape. The density of pollution particles was 2.8×10^3 kg/m^3. The flow field inlet was set as ''velocity-inlet'', which was used to enter the wind with different speed, the pollution particles with different diameters. Based on the characteristic of air flow field, the turbulent intensity of ''velocity-inlet'' was 5%. The acceleration of gravity was 9.81 m/s^2.

E. PARTICLE SIZE AND WIND SPEED

Atmospheric particulate matter is generally divided into three mode distributions: Aitken mode ($dp \leq 0.08$ μm), accumulation mode ($0.08< dp \leq 2$ μm) and coarse particle mode ($dp > 2$ μm) [15]. The pollution particles of Aitken mode form larger diameter particles by chemical reaction, resulting in a short time in the air for the particles of Aitken mode; The accumulated modal particles are mainly composed of organic matter, metal and various ions, which can be suspended in the air for a long time and can be transmitted in the air for a long distance; The coarse particles ($dp > 2$ μm) are mainly composed of dust and coal ash, which are transported in the air for several hundred meters to several tens of kilometres, landed on the ground by sedimentation [16].

The size distribution of atmospheric precipitation particles in winter is as follows: the volume fraction of particles with the size of 10∼50 μm is 51.2%, the pollution particles with the size of 2.5∼10 μm is 35.1%, with the pollution particles with less than 2.5 μm is 11.2%, and the volume percentage of pollution particles larger than 50 μm is 2.5% [21]. It is found that the diameter distribution of pollution particles on the insulator surface of high-voltage transmission line mainly distribute 5 ∼ 50 μm [22].

In order to obtain the particle size distribution on the insulator surface, the microscopic morphology of the actual

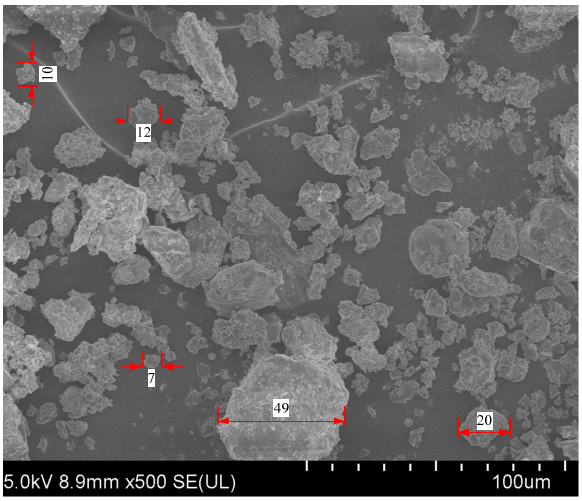

FIGURE 6. SEM image of pollution particles on the insulator surface.

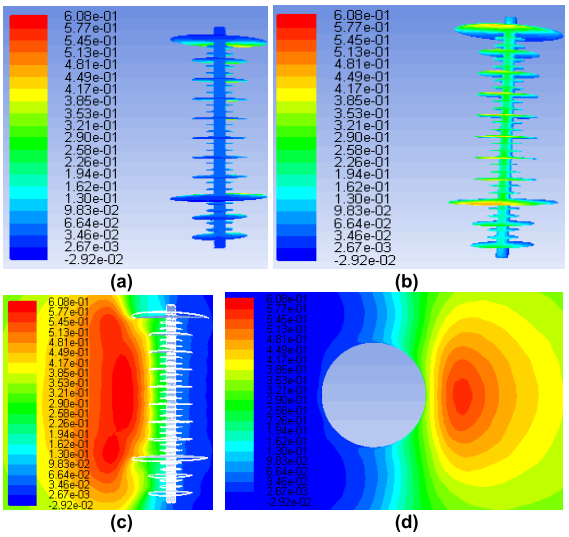

FIGURE 7. The pressure nephogram insulator surface and pressure distribution of air flow field (a) leeward side. (b) windward side. (c) y-z section. (d) x-y section.

polymer insulator surface was observed. Figure 6 shows the scanning electron microscope (SEM) image of pollution particles. It is found that the particle size deposited on the insulator surface is mainly between 1 μm and 50 μm. The pollution particles are mostly irregular coarse particles, which are mainly produced by the mechanical force, including wind dust and building dust. This paper mainly considers the collision characteristics between the pollution particles and the insulator surface, so the shape of pollution particles is neglected, and the pollution particles are set to the spherical particles. The accumulation characteristics of pollution particles with 1 μm $\sim$ 50 μm are analysed according to the actual operation of outdoor insulators.

III. RESULTS AND DISCUSSION

A. PRESSURE DISTRIBUTION ON THE INSULATOR SURFACE

Figure 7 shows the pressure nephogram on the insulator surface and the pressure distribution of air flow field at 1 m/s. The pressure distribution is a physical parameter that characterizes the force generated by the air flow field, and it can represent the energy of per unit volume of air [23]. The pressure nephogram can be obtained to characterize the pressure distribution of insulator surface, which is helpful to analyse the collision between pollution particles and insulator surface.

The red part of pressure nephogram indicates that the pollution particles easily collide with the insulator surface, the green and blue part indicates that the pollution particles bypass the insulator surface. The largest sheds of outdoor insulator on the windward side are subjected to the mainly force generated by air flow field (Figures 7a and 7b). Due to the influence of the largest sheds and insulator mandrel, the pressure distribution of air flow field on leeward side is smaller than that on windward side (Figures 7c and 7d).

The distribution of air flow field and the pressure on the insulator surface has a significant relationship with the wind velocity in the nature [24]. In the actual operating transmission line, the wind velocity around the insulator has a large variation range, which can influence the pressure of outdoor insulator on both windward and leeward side. In this paper, to obtain the pressure changes on the windward and leeward side of insulator surface, different wind speed (from 1 m/s to 22 m/s) were considered.

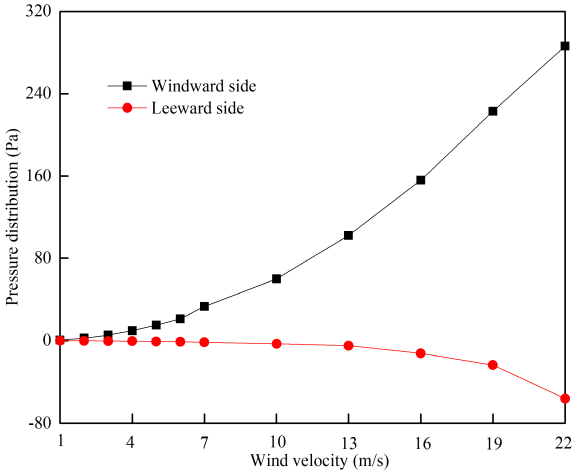

FIGURE 8. The pressure distribution of outdoor insulators under different wind velocity (windward and leeward side).

As shown in Figure 8, the pressure has positive and negative values, which is relative to the standard atmospheric pressure (101325 Pa). When the pressure is higher than the reference value, the pressure on the insulator surface is positive. Otherwise, it is negative. The insulator is subjected to the positive pressure on the windward side and the negative pressure on the leeward side. When the wind speed in air flow field is significantly weak, the difference between the positive

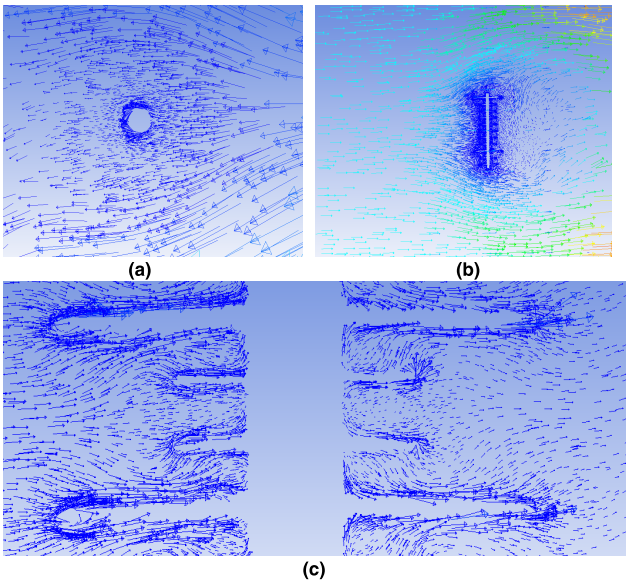

FIGURE 9. The velocity vector around the outdoor insulator at the wind velocity of 1 m/s (a) x-y section. (b) y-z section. (c) velocity vector around insulator (left: windward side, right:leeward side).

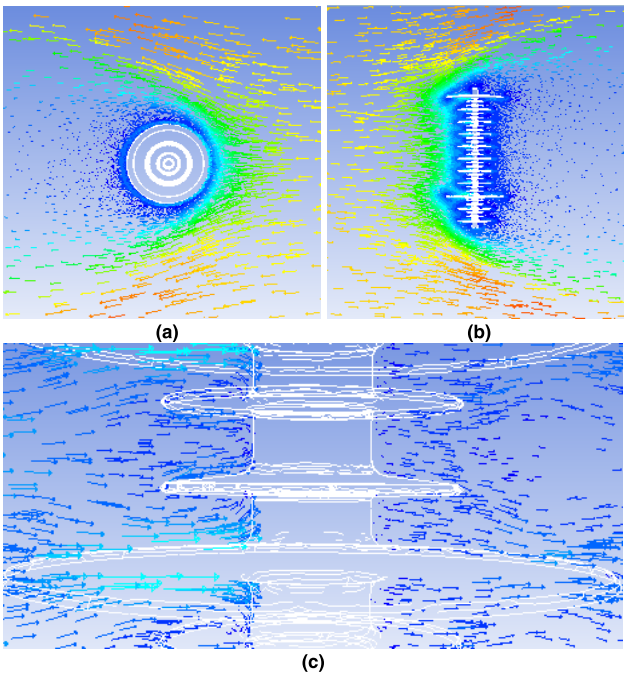

FIGURE 10. The velocity vector around outdoor insulator at the wind velocity of 10 m/s. (a) x-y section. (b) y-z section. (c) velocity vector around insulator (left: windward side, right:leeward side).

and negative pressure is very small, indicating that the air flow around the insulator surface and the collision between pollution and insulator surface are very weak. As the wind speed increases, the positive pressure shows an increasing trend, while the negative pressure shows a downward trend, resulting in the pressure difference of insulator surface to improve increasingly. The influence of wind speed on the flow field around the insulator is more and more obvious to carry more pollution particles on the insulator surface. On the windward side of the insulator, the pollution particle directly collides with the insulator surface, causing the accumulation of pollution particle. Because of the negative pressure and air swirl on the leeward side, the velocity of air flow is slow, resulting in the accumulation of pollution particle more severely.

B. VELOCITY VECTOR AROUND THE OUTDOOR INSULATOR

At low wind velocity, as the air flow through cylindrical obstacles, the air flow appeares as a streamlined flow layer [25]. With the improvement of wind velocity, the velocity gradient of airflow on the surface is large enough to destroy the streamlined flow layer and the air swirl with low velocity will appear on the leeward side of the obstacle [26]. The velocity vector can be considered to describe the flow field distribution around the insulator.

Figures 9 and 10 show the velocity vector of outdoor insulator in different views at 1 m/s and 10 m/s respectively. The maximum velocity of air flow field is in the crosswind side of outdoor insulator. The air flow velocity on the windward side is larger than that on the airflow velocity of leeward side. The mandrel and largest shed of insulator prevent the flow of air, resulting in the air swirl with low velocity between two large sheds on the windward and leeward side. There is an upward flow of air between the sheds on windward side, causing the collision between the pollution particles and the insulator surface. On the leeward side, the velocity of air flow field is small, and the air swirl exists clearly to make collision rate increase significantly (Figures 9c and 10c).

Comparing the velocity vector of the air flow around the insulator surface, it can be obtained that the different wind velocities make the size of air swirls change a lot. The velocity of air flow on the windward side at 10 m/s is bigger than that at 1 m/s, resulting in the collision rate and pressure of insulator surface increase. The velocity vector around insulator sheds on the leeward and windward side has a weakly difference at 1 m/s. As the wind velocity increases, there is a significant air swirl on the leeward side of insulators, which makes air flow velocity decrease and the collision rate of pollution particles increase (Figure 10c).

C. EFFECTS OF THE PARTICLE DIAMETER ON THE COLLISION RATE

The diameter of pollution particles affects the gravity and inertia of particles, which makes the movement characteristic of pollution particles around the insulator changes a lot [27]. In this paper, the particle concentration at 150 μ g/m^3 (14928 particles per square meter), the particle diameter (1 μm $\sim$ 50 μm), the hanging angle (0°), the air humidity (relative humidity of 50%) and wind velocity (1 m/s $\sim$ 22 m/s) were selected to investigate the collision rate.

When the pollution particles are from 1 μm to 10 μm, the pollution particles can be suspended in the air and flow with

the air at various wind speeds, resulting that the accumulation characteristics of pollution particles can be analysed at the wind speed of 1 m/s to 22 m/s. When the pollution particles are larger than 10 μm, the pollution particles are sediments, which will fall to the ground under the action of gravity, and can only be blown into the air under the action of strong wind. Therefore, the wind speed of the particle size larger than 10 μm is discussed for the condition of 7 m/s to 22 m/s.

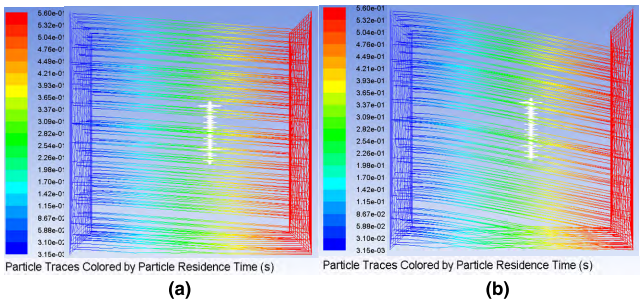

FIGURE 11. The movement trajectory of pollution particles at 10. m/s. (a) Pollution diameter at 5 μm. (b) Pollution diameter at 30 μm.

Figure 11 shows the movement trajectory of different pollution particles at the wind velocity of 5 m/s. When the pollution particles are in the lower part of the flow field inlet, they will fall into the bottom of flow field before reaching the insulator surface. Due to the influences of gravity and fluid drag force, pollution particles fall in the trajectory of the horizontal projectile motion (Figure 11a). When the pollution particles are close to the insulator surface, some particles collide with insulator, but most of them following the air flow bypass the insulator surface. As the particle diameter increases, the trajectory of the particles changes from the horizontal motion to the oblique parabolic motion, resulting in an increasing collision area between the pollution particles and the insulator sheds. Because of the gravity, the movement angle of particles changes, resulting in an increase in the collision rate.

When the pollution particles are less than 10 μm, the changing trends of collision rate with increasing of particle diameter at different wind velocity are shown in Figure 12a. With the increase in particle diameter, the collision rate between pollution particle and insulator surface shows the increasing tendency, which is because that the sedimentation effect of the pollution particles following gravity has a great influence on the collision rate. As the gravity of pollution particles increases, the trajectory of the particles changes from horizontal motion to oblique parabolic motion, resulting in an increasing probability of collision between the pollution particles and the insulator sheds.

The changing trends of collision rate at different wind velocity are shown in Figure 12b. When the diameter of pollution particles is between 10 and 50 μm, with the increase in particle diameter, the collision rate between particle and insulator surface shows a tendency to increase. Because the pollution particle diameter increases, the gravity and inertia

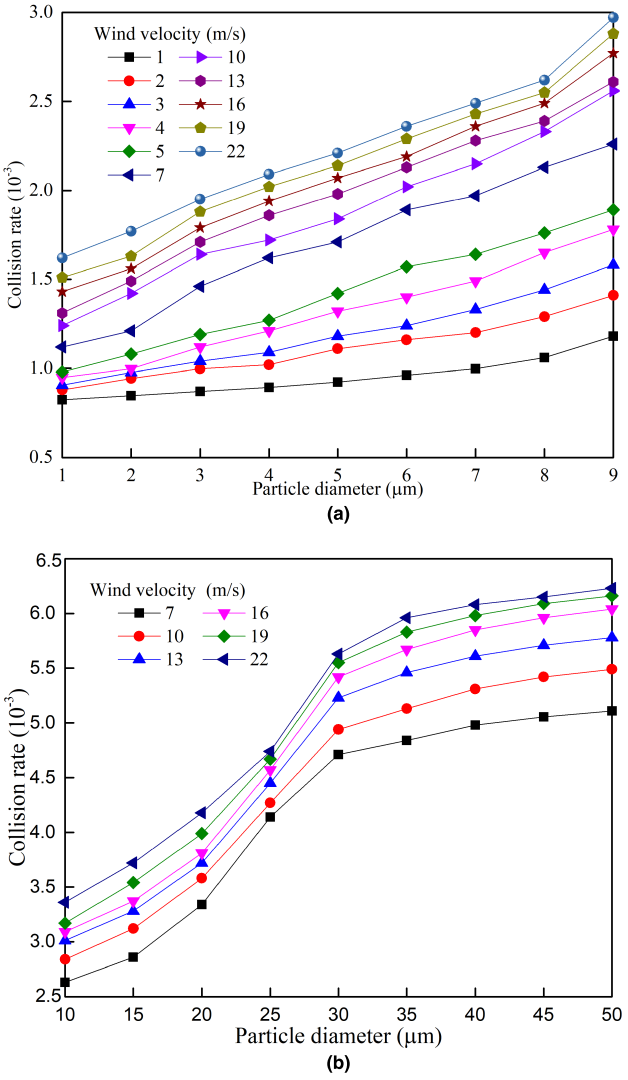

FIGURE 12. The collision rate of pollution particles with different diameters at different wind velocities. (a) Collision rate of pollution particle with smaller diameter (less than 10 μm). (b) Collision rate of pollution particle with high diameter (10∼50 μm).

of particles become large, so that pollution particles moving to insulator surface are not easy to bypass the outdoor insulators, resulting in pollution particles directly collide with insulator surface. When the wind speed is 7 m/s, the influence of inertia on particle motion is gradually weakened as the particle size increases, resulting in a slower increase in collision rate.

D. EFFECTS OF THE PARTICLE CONCENTRATION ON THE COLLISION RATE

The increasing concentration of pollution particles makes more pollution particles accumulate on the insulator surface, resulting in the higher flashover accident of outdoor insulators [28]. PM10 is one of the important indicators for characterizing the level of air pollution, which varies from 30 to 260 μ g/m^3 in different cities [29].

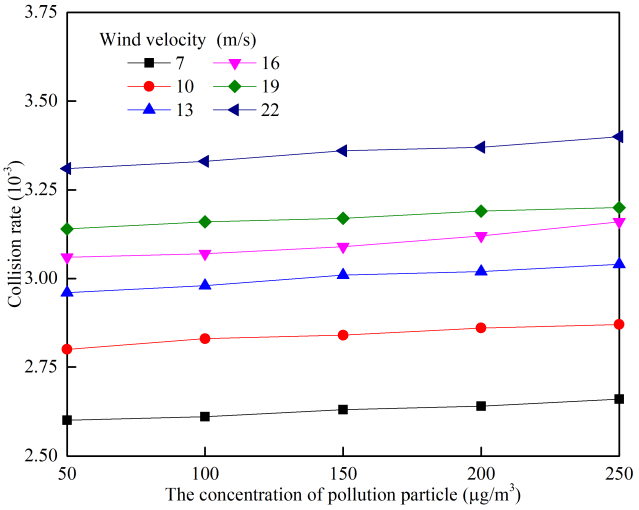

FIGURE 13. The collision rate of particles in different particle concentrations and wind velocities.

In this paper, the particle diameter (10 μm), the wind velocity (7 m/s $\sim$ 22 m/s), the hanging angle (0°), the air humidity (relative humidity of 50%) and the particle concentration (50 μ g/m^3 $\sim$ 250 μ g/m^3) were selected to study the collision rate between the particle and the insulator surface. In the simulation, the particle concentration is transformed into the emission amount of the pollution particles per square meter of the inlet surface, which is 14928, 29856, 44784, 59712, 74640 per square meter respectively.

As the concentration of pollution particles increases, the collision rate between the pollution particles and the insulator surface increases slightly, as shown in Figure 13. Although the collision rate changes weakly with the increase in the particle concentration, the collision number is multiplied, resulting in a significant increase in the amount of pollution particles on the insulator surface. This is because the high concentration of pollution particles increases the probability of collision between the pollution particles and insulator surfaces. At the same wind velocity, more pollution particles move in the air under the fluid drag force, colliding with the insulator surface, so the collision rate is slightly increased. For the actual operating insulator, the amount of pollution particles on the insulator surface is larger in the area with high concentration of pollution particles.

E. EFFECTS OF THE WIND VELOCITY ON THE COLLISION RATE

In different meteorological environments, the wind velocity has a significant influence on the movement trajectory and accumulation of pollution particles [30]. In this paper, the concentration of pollution particle at 150 μ g/m^3 (14928 particles per square meter), the wind velocity of air flow field (1 m/s to 22 m/s), the hanging angle (0°) air humidity (relative humidity of 50%) and particle diameter (1 μm to 50 μm) were set to investigate the movement trajectory of pollution particles.

The collision rate of pollution particles with different diameters and wind velocity is shown in Figure14. When the particle diameter is small (1 μm to 9 μm), the collision rate of pollution particles increases as the wind speed increases (Figure 14a). When the wind velocity is less than 7 m/s, the collision rate increases significantly with the increase in the wind velocity. This is because as the wind speed increases, the pollution particles will hardly bypass the insulator surface, causing the pollution particles directly collide with the windward side of insulator surface to increase the collision rate of the pollution particles. When the wind speed is higher than 7 m/s, the collision rate increases slowly with the increase in the wind velocity. This is because as the wind velocity increases, the air swirls are generated on the leeward side of insulator surface, causing the slow air flow velocity. Therefore, the pollution particles collide with the leeward side of insulator surface, resulting in an increase in the collision rate of pollution particles.

When the particle diameter is big (10 μm to 50 μm), the changing trend of collision rate is shown in Figure 14b. Compared with the small pollution particles, the collision rate of large pollution particles increases greatly at the same wind velocity (Figures 14a and 14b). This is because as the wind increases, the large pollution particles are affected by the fluid drag force, turbulent diffusion and the gravity force, resulting in a gradual increase in the collision rate of pollution particles. As the wind velocity increases, the influences of fluid drag force and gravity force on the trajectory of pollution particles is gradually weakened, and the air swirl becomes the main factor affecting the slow increase in the collision rate.

F. EFFECTS OF HANGING ANGLE ON THE COLLISION RATE

In the operating transmission line, there are a variety of suspension methods for outdoor insulator, such as "V", "Λ" and "II" types. The hanging angle between two insulators for these suspension methods affects the accumulation characteristic of pollution particle [31], [32]. In order to simplify the calculation model, one side of "V" type insulator was established to analyze the influence of hanging angle on the collision rate. When the angle of "V" type insulator is 30°, the hanging angle of each side is 15°, as shown in Figure 15. The hanging angle of insulator (0° $\sim$ 60°), particle diameter (1 μm $\sim$ 22 μm), the concentration of pollution particle (150 μ g/m^3), air humidity (relative humidity of 50%) and wind velocity (10 m/s) were set to study the collision rate of pollution particles.

The pressure nephogram of "V" type insulator in different hanging angles is shown in Figure 16. When the hanging angle is small, the insulator sheds and mandrel are subjected to the main pressure of air flow. With increasing the angle from 15° to 45°, the blocking effect of sheds make the pressure of insulator mandrel is smaller. In the different hanging angles, the velocity vector and the flow of air swirl change remarkably, resulting in the pressure difference on the insulator surface.

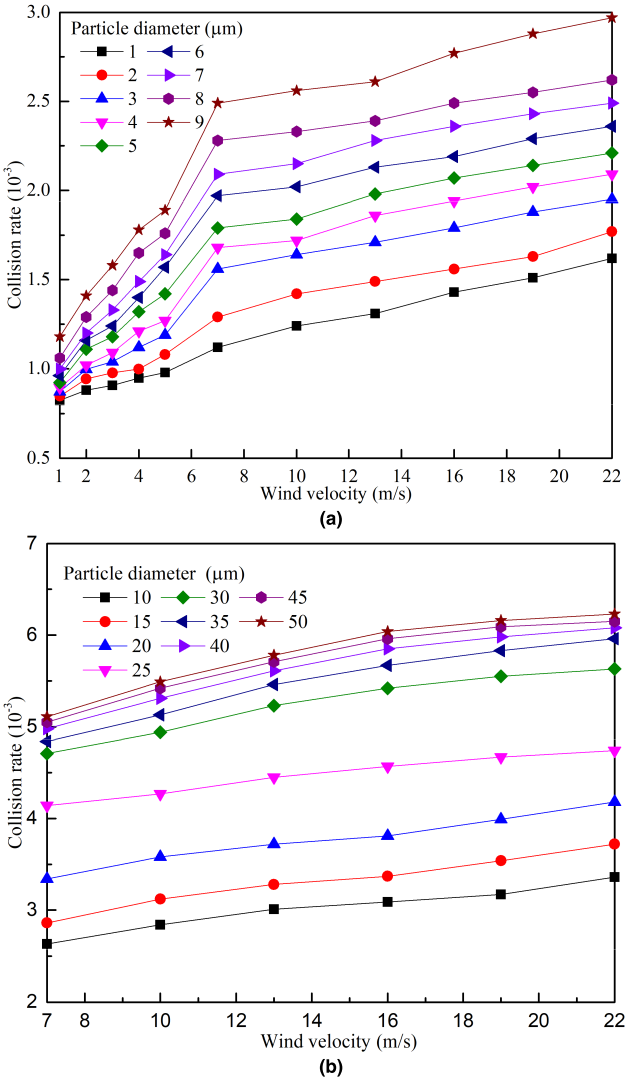

FIGURE 14. The collision rate of pollution particles under the conditions of different wind velocities and particle diameters. (a) Collision rate of pollution particle with smaller diameter. (b) Collision rate of pollution particle with high diameter.

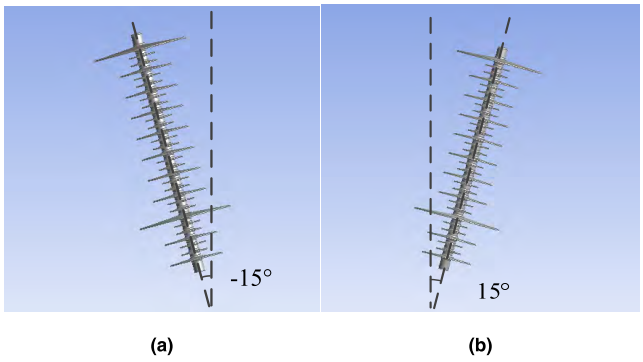

FIGURE 15. 3-D model of "V" type insulator (included angle of 30°). (a) Hanging angle at −15°. (b) Hanging angle at 15°.

The collision rate of "V" type insulator in different hanging angles and particle diameters is shown in Figures 17 and 18. When the hanging angle increases from

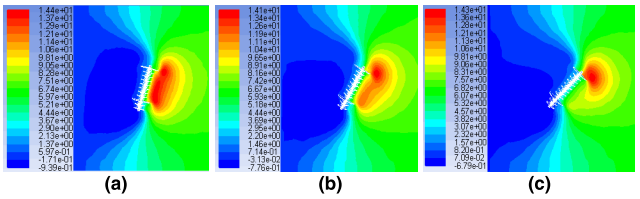

FIGURE 16. The pressure nephogram of outdoor insulator in different hanging angles. (a) (15°). (b) (30°). (c) (45°).

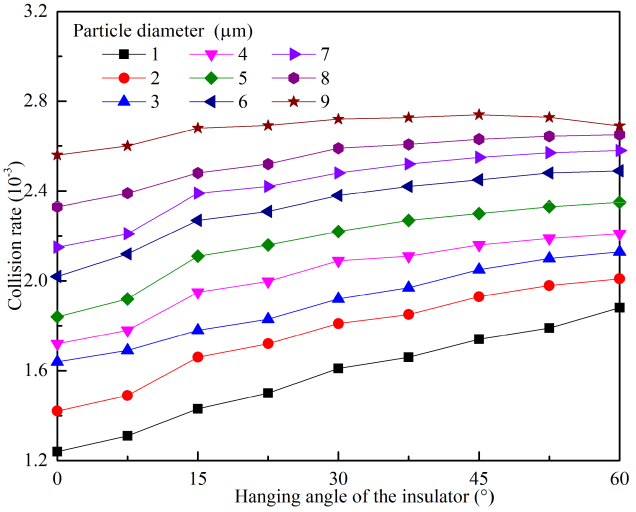

FIGURE 17. Collision rate of pollution particle with smaller diameter in relation to the hanging angle from 0° to 60°.

0° to 60°, the collision rate of particles shows the increasing tendency, as shown in Figure 17. The pollution particles with smaller size are mainly affected by the fluid drag force at the wind velocity of 10 m/s to make the movement trajectory of pollution particles is parallel to the shed surface, resulting in the smaller collision rate between pollution particle and insulator surface. As the inclined angle of insulator sheds increases, the windward area of insulator surface increases significantly, so that the collision probability between the pollution particles and the insulator sheds is enhanced.

For the particle diameter from 9 μm to 50 μm, when the hanging angle increases from 0° to 30°, the collision rate shows the increasing tendency with the angle higher than 30°, but then shows the decreasing tendency (Figures 17 and 18). As the inclined angle of insulator increases, the gravity force and the inertia play the significant role to cause the pollution particle collide with the insulator surface directly, resulting in the increase in the collision rate. Due to the specific structure of polymer insulator, when the hanging angle reaches 30°, the largest shed of insulator will prevent the movement of pollution particles, which makes the collision rate of the particle decrease.

G. EFFECTS OF AIR HUMIDITY ON THE COLLISION RATE

When the humidity in the air is large, a large amount of water vapor exists in the air, which has an important influence on the

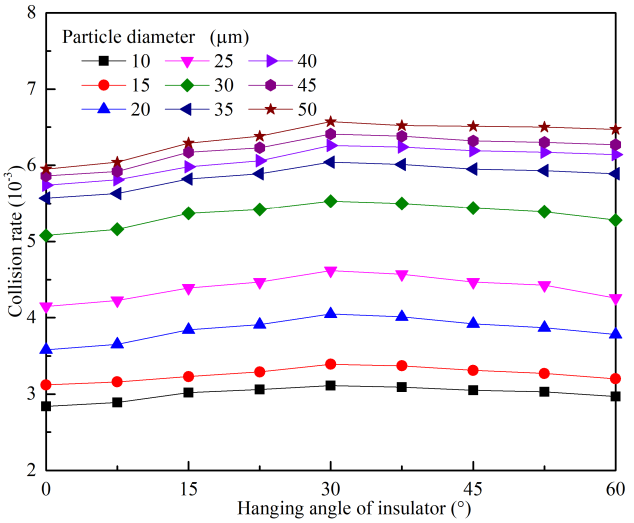

FIGURE 18. Collision rate of pollution particle with high diameter in relation to the hanging angle from 0° to 60°.

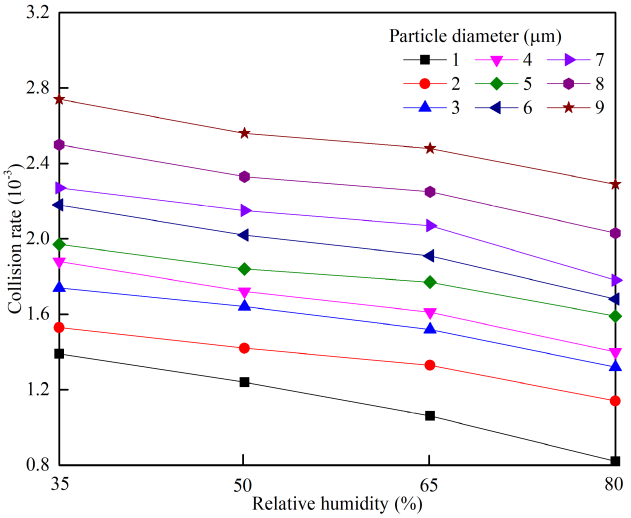

FIGURE 19. Collision rate of pollution particle with smaller diameter in different air humidity and particle diameter.

flow of pollution particles. In this paper, the influence of air humidity on the collision rate of pollution particles is studied by using gas-liquid two-phase flow, and the air humidity is represented by different liquid ratios of air flow field. Relative humidity refers to the percentage of water vapor pressure in air to saturate water vapor pressure at the same temperature, and the distribution range of relative humidity in air is mainly between 30% and 80% [33], [34]. The particle diameter (1 μm to 22 μm), the hanging angle (0°), the particle concentration (150 μ g/m^3), air humidity (relative humidity of 35%, 50%, 65%, 80%) and wind velocity (10 m/s) were set to study the collision rate of pollution particles. In the simulation, to characterize the water content in the air under different air humidity, the relative humidity is converted into the absolute humidity, which is the weight of water contained per cubic meter of air.

For the pollution particles with smaller diameter, it is greatly affected by the change of air humidity, and the collision rate of pollution particles decreases significantly with the increase in air humidity, as is shown in Figure 19a. When the particle diameter is in the range of 1 μm to 9 μm, as the humidity increases, the pollution particles with smaller diameter will be prevented by the water vapor during the movement. And the scattering phenomenon will appear during the pollution particles moving to the insulator surface, resulting in the decrease in the collision rate.

When the particle diameter is in the range of 10 μm to 50 μm, the collision rate decreases as the humidity increases, but the reduced number of collision rate is less than that of the pollution particles with small diameter, as shown in Figure 20. This is because as the particle diameter increases, the gravity force and the inertia of particles are also gradually increased, so that the water vapor in the air has less influence on the movement of the large-sized pollution particles.

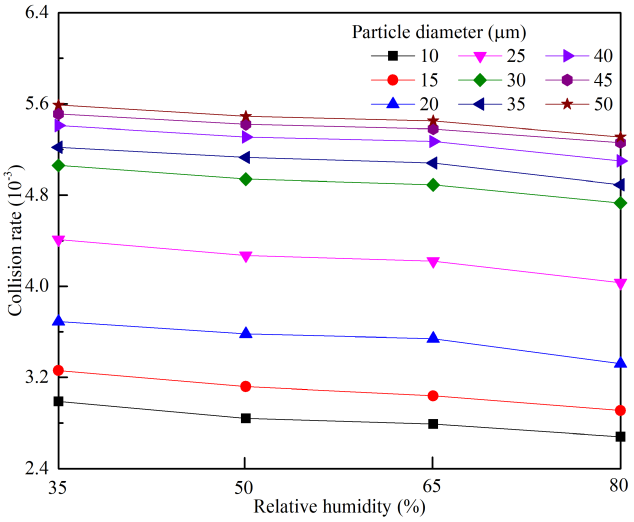

FIGURE 20. Collision rate of pollution particle with high diameter in different air humidity and particle diameter.

IV. CONCLUSION

In this paper, the influencing factors of wind velocity, the concentration of pollution particles, the particle diameter and the suspension method of outdoor insulator were analyzed to investigate the accumulation characteristics of pollution particles. The pressure nephogram of polymer insulator, the velocity vector of air flow field, movement path of pollution particles and the collision rate were obtained. The main conclusions are as follows.

(1) When the wind velocity is significantly weak, the difference between the positive and negative pressure on the insulator surface is very small. As the wind velocity increases, the positive pressure on the insulator surface shows an increasing trend, while the negative pressure shows a downward trend.

(2) With the increase in particle diameter, the collision rate between pollution particle and insulator surface shows the increasing tendency. When the diameter of the pollution particles is small, the easier the particles follow the airflow to bypass the insulator surface without colliding with it, causing the smaller collision rate between insulator surface and pollution particles. While the collision rate of pollution particles significantly increases with the increase in particle diameter.

(3) When the wind velocity is less than 7 m/s, the pollution particles directly collide with the windward side of insulator surface, resulting in the collision rate of pollution particles significantly increases with the increase in wind velocity. When the wind speed is higher than 7 m/s, the air swirls are generated on the leeward side of insulator surface, causing the collision rate of pollution particles slowly increases with the increase in the wind velocity.

(4) As the concentration of pollution particle increases, the collision rate between insulator surface and pollution particles shows the increasing tendency at different wind velocities.

(5) When the particle diameter is in the range of 1 μm to 8 μm, with the hanging angle of ''V'' type insulator from 0° to 60°, the collision rate of pollution particles shows the increasing tendency. When the particle diameter is in the range of 9 μm to 50 μm, with increasing the insulator angle of ''V'' type from 0° to 30°, the collision rate of pollution particles shows the increasing tendency, but shows the decreasing tendency with the hanging angle from 30° to 60°.

(6) As the air humidity increases, the water vapor in the air prevents the movement of pollution particles, resulting in a decrease in the collision rate of pollution particles. As the pollution particles diameter increases, the influence of air humidity on the collision rate is gradually weakened.

REFERENCES

[1] X. Zhangm J. Zhu, S. Bu, Q. Li, V. J. Terzija, and S. M. Rowland, ''The development of low-current surface arcs under clean and salt-fog conditions in electricity distribution networks,'' *IEEE Access*, vol. 6, pp. 15835–15843, 2018.

[2] Y. Guo, X. Jiang, Y. Liu, Z. Meng, and Z. Li, ''AC flashover characteristics of insulators under haze–fog environment,'' *IET Gener., Transmiss. Distrib.*, vol. 10, no. 14, pp. 3563–3569, Nov. 2016.

[3] B. Gao *et al.*, ''The movement characteristics of charged haze particles in ionized field and its influence on contamination of insulator,'' *IEEE Trans Magn.*, vol. 54, no. 3, Mar. 2018, Art. no. 7203304.

[4] Y. Liu *et al.*, ''Identification of lightning strike on 500-kV transmission line based on the time-domain parameters of a traveling wave,'' *IEEE Access*, vol. 4, pp. 7241–7250, 2016.

[5] Z. Zhang *et al.*, ''Influence factors in contamination process of XP-160 insulators based on computational fluid mechanics,'' *IET Gener., Transmiss. Distrib.*, vol. 10, no. 16, pp. 4140–4148, Dec. 2016.

[6] K. Takasu, T. Shindo, and N. Arai, ''Natural contamination test of insulators with DC voltage energization at inland areas,'' *IEEE Trans. Power Del.*, vol. PWRD-3, no. 4, pp. 1847–1853, Oct. 1988.

[7] L. Li, Y. Jiang, M. Lu, Z. Liu, K. Hua, and Z. Li, ''Study on the difference of chemical composition of insulator contamination on UHV-AC and -DC transmission lines,'' *IET Sci. Meas. Technol.*, vol. 12, no. 1, pp. 17–24, Jan. 2018.

[8] Z. Zhang, J. You, J. Zhao, Y. Cheng, X. Jiang, and Y. Li, ''Contamination characteristics of disc-suspension insulator of transmission line in wind tunnel,'' *IET Gener. Transmiss. Distrib.*, vol. 11, no. 6, pp. 1453–1460, Apr. 2017.

[9] J. G. Wang, K. Wang, M. Zhou, L. Zhao, S. Yao, and C. Fang, ''The natural contamination of XP-70 insulators in Shenzhen, China,'' *IEEE Trans. Dielectr. Electr. Insul.*, vol. 23, no. 1, pp. 349–358, Feb. 2016.

[10] Z. Zhang, D. Zhang, X. Jiang, and X. Liu, ''Study on natural contamination performance of typical types of insulators,'' *IEEE Trans. Dielectr. Electr. Insul.*, vol. 21, no. 4, pp. 1901–1909, Aug. 2014.

[11] Y. Lv, J. Li, X. Zhang, G. Pang, and Q. Liu, ''Simulation study on pollution accumulation characteristics of XP13-160 porcelain suspension disc insulators,'' *IEEE Trans. Dielectr. Electr. Insul.*, vol. 23, no. 4, pp. 2196–2206, Aug. 2016.

[12] O. E. Gouda and A. Z. El Dein, ''Simulation of overhead transmission line insulators under desert environments,'' *IET Gener. Transmiss. Distrib.*, vol. 7, no. 1, pp. 9–13, Jan. 2013.

[13] A. C. Baker *et al.*, ''Insulator selection for AC overhead lines with respect to contamination,'' *IEEE Trans. Power Del.*, vol. 24, no. 3, pp. 1633–1641, Jul. 2009.

[14] C. Zhang, J. Hu, J. Li, D. Liu, L. Wang, and M. Lu, ''Experimental study on the contamination deposition characteristics of insulators in a fog–haze environment,'' *IET Gener., Transmiss. Distrib.*, vol. 12, no. 2, pp. 406–413, Jan. 2018.

[15] A. Eldering and R. M. Glasgow ''Short-term particulate matter mass and aerosol-size distribution measurements: Transient pollution episodes and bimodal aerosol-mass distributions,'' *Atmos. Environ.*, vol. 32, no. 11, pp. 2017–2024, 1998.

[16] H. Wang, Z. Sun, H. Li, Y. Gao, J. Wu, and T. Cheng, ''Vertical-distribution characteristics of atmospheric aerosols under different thermodynamic conditions in Beijing,'' *Aerosol Air Qual. Res.*, vol. 18, no. 11, pp. 2775–2787, Mar. 2018.

[17] L. Wang, B. Cao, H. Mei, C. Zhao, and Z. Guan, ''Effects of natural contamination components on the surface conductivity under saturated moisture,'' *IEEE Trans. Dielectr. Electr. Insul.*, vol. 24, no. 5, pp. 2945–2951, Oct. 2017.

[18] J. Wardman, T. Wilson, S. Hardie, and P. Bodger, ''Influence of volcanic ash contamination on the flashover voltage of HVAC outdoor suspension insulators,'' *IEEE Trans. Dielectr. Electr. Insul.*, vol. 21, no. 3, pp. 1189–1197, Jun. 2014.

[19] S. A. Morsi and A. J. Alexander, ''An investigation of particle Trajectories in two-phase flow systems,'' *J. Fluid Mech.*, vol. 55, no. 2, pp. 193–208, Sep. 1972.

[20] L. Li, Y. Li, M. Lu, Z. Liu, C. Wang, and Z. Lv, ''Quantification and comparison of insulator pollution characteristics based on normality of relative contamination values,'' *IEEE Trans. Dielectr. Electr. Insul.*, vol. 23, no. 2, pp. 965–973, Apr. 2016.

[21] S.-L. Wang, F.-H. Chai, and Y.-H. Zhang, ''Analysis on the sources and characters of particles in Chengdu,'' *Scientia Geographica Sinica*, vol. 24, no. 4, pp. 488–492, Aug. 2004.

[22] H.-Z. Li, Y.-K. Wang, G. Liu, Y.-F. Lin, Y.-P. Liu, and X. Xu, ''Discussing about the equivalent model and particles size distribution of pollution prticles of power system external insulation,'' *Insulators Surge Arresters*, vol. 1, pp. 34–38, Feb. 2013.

[23] N. Dhahbi-Megriche, W. Arfaoui, and A. Beroual, ''Computer package for selecting high voltage insulators for different contamination conditions,'' *IEEE Trans. Dielectr. Electr. Insul.*, vol. 20, no. 4, pp. 1428–1435, Aug. 2013.

[24] H. Su, Z. Jia, Z. Sun, Z. Guan, and L. Li, ''Field and laboratory tests of insulator flashovers under conditions of light ice accumulation and contamination,'' *IEEE Trans. Dielectr. Electr. Insul.*, vol. 19, no. 5, pp. 1681–1689, Oct. 2012.

[25] A. Banik, S. Dalai, and B. Chatterjee, ''Autocorrelation aided rough set based contamination level prediction of high voltage insulator at different environmental condition,'' *IEEE Trans. Dielectr. Electr. Insul.*, vol. 23, no. 5, pp. 2883–2891, Oct. 2016.

[26] S. Li, X. Liang, Y. Gao, Y. Liu, Y. Yin, and Z. Li, ''A modified 5000 h test procedure for silicone rubber insulator based on contamination and hydrophobicity change simulation,'' *IEEE Trans. Dielectr. Electr. Insul.*, vol. 24, no. 3, pp. 1818–1828, Jun. 2017.

[27] Y. Jiang, S. G. McMeekin, A. J. Reid, A. Nekahi, M. D. Judd, and A. Wilson, ''Monitoring contamination level on insulator materials under dry condition with a microwave reflectometer,'' *IEEE Trans. Dielectr. Electr. Insul.*, vol. 23, no. 3, pp. 1427–1434, Jun. 2016.

[28] F. Zhang, L. Wang, Z. Guan, and M. Macalpine, "Influence of composite insulator shed design on contamination flashover performance at high altitudes," *IEEE Trans. Dielectr. Electr. Insul.*, vol. 18, no. 3, pp. 739–744, Jun. 2011.
[29] L. Morawska, S. Thomas, N. Bofinger, D. Wainwright, and D. Neale, "Comprehensive characterization of aerosols in a subtropical urban atmosphere: Particle size distribution and correlation with gaseous pollutants," *Atmos. Environ.*, vol. 32, nos. 14–15, pp. 2467–2478, Aug. 1998.
[30] N. Dhahbi-Megriche and A. Beroual, "Self-consistent multi-arcs dynamic model for high voltage polluted insulators," *IEEE Trans. Dielectr. Electr. Insul.*, vol. 23, no. 5, pp. 2899–2907, Oct. 2016.
[31] X. Jiang, Y. Guo, Z. Meng, Z. Li, and Z. Jiang, "Additional salt deposit density of polluted insulators in salt fog," *IET Gener. Transmiss. Distrib.*, vol. 10, no. 15, pp. 3691–3697, Nov. 2016.
[32] S. S. Shunmugam, N. Vasudev, K. N. Ravi, and K. A. Venkatesh, "Influence of profile on the pollution performance of cap-and-pin insulators-an experimental study," *IEEE Elect. Insul. Mag.*, vol. 32, no. 6, pp. 20–28, Dec. 2016.
[33] Z. Zhang, J. You, D. Zhang, X. Jiang, J. Hu, and W. Zhang, "AC flashover performance of various types of insulators under fan-shaped non-uniform pollution," *IEEE Trans. Dielectr. Electr. Insul.*, vol. 23, no. 3, pp. 1760–1768, Jun. 2016.
[34] C. Zhang, L. Wang, and Z. Guan, "Investigation of DC discharge behavior of polluted porcelain post insulator in artificial rain," *IEEE Trans. Dielectr. Electr. Insul.*, vol. 23, no. 1, pp. 331–338, Feb. 2016.

YONG LIU (M'12) was born in Tangshan, China, in 1980. He received the M.E. and Ph.D. degrees in electrical engineering from Tianjin University, China, in 2006 and 2009, respectively, where he has been a Lecturer and then an Associate Professor with the School of Electrical Engineering and Automation, since 2009. From 2014 to 2015, he was a Research Fellow with the NSERC/Hydro-Quebec/UQAC Industrial Chair on Atmospheric Icing of Power Network Equipment, Canada. His current research interests include ageing evaluation and performance monitoring of outdoor insulators under various atmospheric conditions.

XIANGHUAN KONG was born in Henan, China, in 1995. He received the B.Sc. degree from the Harbin University of Science and Technology, Harbin, China, in 2017. He is currently pursuing the M.S. degree with the Department of Electrical Engineering, Tianjin University. His current research interest includes optimization evaluation of insulation structure of transmission lines.

BOXUE DU (M'00–SM'04) received the M.E. degree in electrical engineering from Ibaraki University, in 1993, and the Ph.D. degree from the Tokyo University of Agriculture and Technology, in 1996. He was an Associated Professor with the Niigata College of Technology, Japan. He is currently a Professor with the Department of Electrical Engineering, School of Electrical and Information Engineering, Tianjin University, China. His current research interests include dielectric failure mechanisms of polymer insulating materials, electrical insulation technology, and partial discharge measurements. He is a member of IEEJ and a Senior Member of CSEE.

JIN LI (M'17) was born in Tangshan, China, in 1988. He received the B.S. and Ph.D. degrees in electrical engineering from Tianjin University, China, in 2012 and 2017, respectively. He is currently an Associate Professor with the School of Electrical Engineering and Information, Tianjin University. His research interest includes the designing and the improvement of solid dielectrics for HVDC power cable and gas-insulated transmission line.

JINGSHENG SUN was born in Beijing, China, in 1977. He received the M.E. degree from Tianjin University, China, in 2010. He is currently with State Grid Tianjin Electric Power Corporation. His current research interests include management and investigation of power systems.